

Metal-insulator transition in 2D: the role of interactions and disorder

George Kastinakis

*Institute of Electronic Structure and Laser (IESL), Foundation for Research and Technology - Hellas (FORTH),
Iraklio, Crete 71110, Greece**

Dept. of Chemical Engineering, University of Cambridge, Cambridge CB2 3RA, U.K.

(September 7, 2004)

We present a model for the metal-insulator transition in 2D, observed in the recent years. Our starting point consists of two ingredients only, which are ubiquitous in the experiments: Coulomb interactions and weak disorder spin-orbit scattering (coming from the interfaces of the heterostructures in question). In a diagrammatic approach, we predict the existence of a characteristic temperature $T_o = T_o(n, \omega_H)$, n being the density of carriers, and ω_H the Zeeman energy, below which these systems become metallic. This is in very good agreement with experiments, and corroborates the fact that varying n and ω_H are equivalent ways into/out of the metallic regime. The conductivity, calculated as a function of temperature and ω_H in the metallic state, compares favorably to experiment. Moreover, we give an explicit expression for the conventional weak disorder contributions to the conductivity in the frame of our model. We comment on the nature of the transition, and calculate the specific heat of the system.

PACS numbers: 71.30.+h, 72.10.Bg, 72.10.-d, 72.15.Rn

In the last years, a metal-insulator transition has been observed in 2D systems by Kravchenko et al.¹ and others - see e.g.². In high mobility heterostructures, for carrier densities n higher than a critical density $n_c \sim 10^{11} \text{cm}^{-2}$, and at appropriately low temperatures T , of a few degrees Kelvin at *most*, a transition into a metallic state is observed². Moreover, a sufficient increase of the Zeeman energy ω_H of the carriers, through an externally applied magnetic field H , takes the system back into the insulating state². Hamilton et al.³ and Pudalov et al.⁴ have shown that beyond a maximum characteristic n'_c there is a second metal to insulator transition. Further, in the metallic regime, the resistivity is usually fitted very well by the formula - e.g.^{5,2}:

$$\rho_{exp}(T) = \rho_o + \rho_1 \exp[-(T_*/T)^k] , \quad (1)$$

where ρ_o, ρ_1 and T_* depend on n . The exponent k is in the range 0.5 - 1, and is material-dependent.

Ilani et al.⁶ have shown that for $n < n_c$ the insulating state is spatially inhomogeneous. Here, we will not attempt to provide a description of the insulating state. We *only* give a mechanism for the transition and a description of the metallic state. These are based on strong spin-dependent particle-hole correlations, which arise for the appropriate range of n and ω_H , in the frame of a Fermi liquid formulation.

The experimental systems in question have two ubiquitous characteristics. The ratio of the Coulomb energy to the Fermi energy ϵ_F is typically in the range 4-40². The importance of interactions has been decisively demonstrated by Ilani et al.⁶ and Dultz and Jiang⁷, who probed the compressibility in the metallic regime, and found it in agreement with a many-body interacting picture. On the other hand, weak disorder spin-orbit scattering is inadvertently present, coming from the interfaces of the heterostructures in question. These two characteristics constitute our starting point. We note that magnetic spin disorder would have the *same* effect as spin-orbit disorder, in the frame of our model. Strong support for the role of spin-dependent scattering is provided by the expts. of Vitkalov et al.⁸, which show that spin up and down mobilities remain comparable for all H . This is naturally interpreted in terms of strong spin up and down mixing through disorder scattering. Further, Ilani et al.⁹ have demonstrated the existence of localized charged islands in the metallic phase, which can be magnetic. If this is the case, we can assume that these magnetic islands sit on top of the aforementioned spin-orbit impurities. Then the scattering strength of the impurities is enhanced and the metallic behavior is more pronounced - c.f. e.g. eq. (6) for $T_o(n, \omega_H)$ etc.

In the foregoing, we consider the coupling U between opposite spin carriers, and we denote by

$$u \equiv UN_F , \quad (2)$$

the dimensionless coupling, N_F being the density of states at the Fermi level. As usual, we work in the regime $\epsilon_F \tau > 1$ ($\hbar = 1$), ϵ_F being the Fermi energy and τ^{-1} the total impurity scattering rate. As we have shown in¹⁰, in the presence of weak disorder, which includes *spin* scattering, the ladder diagrams in the particle-hole channel give rise to the propagators $A^j(q, \omega_m)$, $j = 0, \pm 1$, obeying the coupled Bethe-Salpeter equations

$$\begin{aligned} A^1 &= U + UD^1 A^1 + UD^0 A^0 , \\ A^0 &= UD^0 A^1 + UD^{-1} A^0 . \end{aligned} \quad (3)$$

The variables q, ω_m , which stand for the momentum and Matsubara energy difference between particle and hole lines respectively, were suppressed. \mathcal{D}^j are given by $\mathcal{D}^{\pm 1} = \mathcal{D}^{1, \pm 1}$, $\mathcal{D}^0 = [\mathcal{D}^{0,0} - \mathcal{D}^{1,0}]/2$, $\mathcal{D}^{j, m_j}(q, \omega_m) = N_F \{Dq^2 + j4\tau_S^{-1}/3\} / \{Dq^2 + j4\tau_S^{-1}/3 + |\omega_m| - im_j\omega_H\}$, with τ_S^{-1} the total spin scattering rate and D the diffusion constant. In Appendix A we present the derivation of these equations and their solution.

What turns out to be of interest here, is the "dynamic limit" $Dq^2 < \omega_m$, where the solution of these eqs. is¹⁰

$$A^j(q, \omega_m) = \frac{K_{uj} + L_{uj}Dq^2 + M_{uj}|\omega_m|}{A_u Dq^2 + B_u |\omega_m| + C_u}, \quad (4)$$

with

$$\begin{aligned} A_u &= 12 - 20u + 15u^2/2 + 6\Omega_H^2, \quad B_u = 4 - 6u + 3u^2/2 + 2\Omega_H^2, \\ C_u &= r[1 - 2u + 3u^2/4 + \Omega_H^2(1 - u^2/4)], \quad K_{u0} = Uru(1 + \Omega_H^2), \quad K_{u1} = Ur(1 - u), \\ L_{u0} &= 2Uu(2 + \Omega_H^2), \quad L_{u1} = 4U(1 - u), \quad M_{u0} = 2Uu(2 + \Omega_H^2), \quad M_{u1} = U(4 - 3u), \end{aligned} \quad (5)$$

where $\Omega_H = 3\omega_H\tau_S/4$ and $r = 4\tau_S^{-1}/3$ ¹¹.

We consider first the case with $\omega_H = 0$. For $u = 2/3 - 2$, $C_u < 0$. For $u \geq 0.845$, $B_u \leq 0$ as well. Then the ratio C_u/B_u is *negative* for $u = 2/3 - 0.845$, with $C_u < 0$ and $B_u > 0$. We interpret this as the onset of strong particle-hole correlations in the spin density channel. For sufficiently low temperatures

$$T < T_o(u, \omega_H) \equiv \frac{|C_u|}{2\pi B_u} \equiv \frac{\omega_o}{2\pi}, \quad (6)$$

a *resonance* occurs - c.f. also eq. (36), which we interpret as driving the second-order transition into the metallic regime - c.f. below. A finite ω_H shrinks the range of u , which allows for this effect, until for high enough ω_H C_u becomes positive definite, and there is *no* transition into the metallic state. The dependence of the transition temperature T_o on u - or equivalently the carrier density - and ω_H are in accordance with experiment^{3,4,12,2}. Namely, the lobe within which the conducting state exists in the ω_H vs. density diagram^{3,4} is easily reproduced by use of the ratio C_u/B_u . Of course, the value of u is determined through the bandstructure by the density n .

We note that additional insertions in the Bethe-Salpeter equations (4) for A^j , such as self-energy diagrams, do not influence the existence of this resonance. Based on the experimental evidence available to date, there is *no* magnetic or superconducting instability involved here. Thus the location of the pole of A^j on the imaginary energy axis is unphysical. In a different approach, Chamon et al.¹³ assume a paired state in the metallic phase. In order to make progress, we assume that in the metallic phase the usual Fermi liquid picture continues to apply, but C_u acquires a small imaginary factor

$$C_u \rightarrow C_u + id, \quad (7)$$

which moves the pole of A^j at a distance off the imaginary axis, thus yielding well-defined metallic contributions to the conductivity. d should be such that the contribution of the diagram B in fig. 1 is substantial for the calculation of the conductivity, as mentioned in Appendix B. Namely the quantity (c.f. eqs. (24) and (36) for R_J and eqs. (10) and (26) for $D(q, \omega)$)

$$Q_{jj'} = \max\{G_R(k, \epsilon)G_A(k, \epsilon)\} |R_j R'_j| \left\{ \text{coefficient of } \sum_q D(q, \omega_T) \right\} = \frac{(2\tau)^2 |R_j R'_j|}{8\pi^2 \tau^2 N_F D}, \quad (8)$$

should not be too small. Also, d should satisfy

$$d = \pm d_o |C_u|^\xi T^\chi, \quad (9)$$

with $0 \leq \xi \leq 1$ ¹⁴, $0 \leq \chi \leq 1$ and $T^\chi d_o(T) \rightarrow 0$ for $T \rightarrow 0$, in order to yield physically meaningful contributions (the sign \pm corresponds to the position of A^j with regards to the main particle-hole lines, as shown in figs. 1-2). In fact, a finite d is consistent with the finite imaginary part of the dephasing rate for *finite* ω - c.f. e.g.¹⁵.

To calculate the conductivity using the renormalized A^j , we proceed as follows. First, relevant processes must take into account the resonance of $A^j(q, \omega)$. For this, diagrams, such as the ones in figs. 1-2, containing pairs of $A^j(q, \omega)$'s with identical q and ω are needed in order to yield the enhancement factor $Q_{jj'}$ of (8) above, which then appears in eq. (11). The diffusons¹⁶

$$D^{j, m_j}(q, \omega_m) = \frac{1}{2\pi N_F \tau^2} \frac{1}{Dq^2 + j4\tau_S^{-1}/3 + |\omega_m| - im_j\omega_H} \quad (10)$$

in between the A^j 's, both provide essential T -dependence and separate the A^j 's from each other. We note that without something separating the 2 A^j 's, they would just reduce into a *single* A^j , and thus not offering this enhancement factor. The diagrams shown in figs. 1-2 yield the maximum contribution around a single diffuson $D(q, \omega_m)$. The reasoning here is similar to a related, but different, calculation in¹⁰.

Summing over all possible spin combinations involving the different A^j 's yields for the total contribution of B

$$B = g\{z_1 F_1 + z_2 F_2\} . \quad (11)$$

Here, $g = \frac{N_F}{2048D^3} \left\{ \frac{T\omega_o}{\pi^3 A_u \epsilon_F^2 d} \right\}^2$, $z_1 = (K_{u1} + M_{u1}\omega_o)^4 + (K_{u0} + M_{u0}\omega_o)^4$, $z_2 = 2(K_{u1} + M_{u1}\omega_o)^2(K_{u0} + M_{u0}\omega_o)^2$, $F_1 = \ln\left(\frac{2\pi T + T_1}{2\pi T}\right)$, $F_2 = \frac{1}{2} \ln\left(\frac{(2\pi T + T_1 + r)^2 + \omega_H^2}{(2\pi T + r)^2 + \omega_H^2}\right)$ and $T_1 = \tau^{-1}$.

Subsequently, we also take into account all the diagrams of the type of fig. 2, with one or two impurity lines passing completely outside the bubbles containing A^j 's. Summing all diagrams from figs. 1 and 2 gives

$$M = \Gamma_1 - \Gamma\Gamma_2 , \quad (12)$$

where $\Gamma = G_R(k, \epsilon_F)G_A(k, \epsilon_F)$, $\Gamma_1 = \alpha\tau^2 B$, $\Gamma_2 = B/(2\pi\epsilon_F\tau)$, with $\alpha = 1 - (2\tau)^2 \left(\frac{4}{9\tau_S^2} + \frac{1}{3\tau_S} \left[\frac{1}{\tau} - \frac{1}{\tau_S} \right] \right)$.

To calculate the conductivity, taking into account M to infinite order, we sum the infinite series, the n -th term of which contains n factors (blocks) M in series, sandwiched between the current vertices of a conductivity bubble :

$$\sigma_M = \frac{2e^2}{m^2} \int d\vec{k} k_x^2 \left\{ \Gamma \sum_{n=1}^{\infty} (\Gamma M)^n = \frac{\Gamma^2 M}{1 - \Gamma M} \right\} . \quad (13)$$

m is the carrier mass. In this way we obtain a M -dependent formula for the total conductivity in the metallic regime

$$\sigma = \sigma_o + \sigma_M = \frac{2N_F e^2 \epsilon_F \pi}{3mS} \left\{ \frac{y_+}{\sqrt{t^2 - y_+}} - \frac{y_-}{\sqrt{t^2 - y_-}} \right\} s_\sigma(T) . \quad (14)$$

Here $y_\pm = (\Gamma_1 \pm S)/2$, $S = \sqrt{\Gamma_1^2 - 4\Gamma_2}$. σ_o is the Drude term. $s_\sigma(T)$ is a smooth analytic function, equal to 1 for $T \leq T_o$ and gradually vanishing for $T > T_o$ ¹⁷. Eq. (14) is a gauge-invariant approximation for the conductivity^{10,18}.

The fit of eq. (14) to the activated exponential in T form for the resistivity of eq. (1), usually fit to the experimental data, is shown in fig. 3. We take $\chi = 1$ - which gives an excellent match with eq. (1) in the "high T " limit, and makes the factor g T -independent - $\xi = 0$ and $d_o = \text{const}$. We plot $\rho(H=0)/\rho_*$, where $\rho = 1/\sigma$ and $\rho_* = 3m\tau/(\pi e^2 N_F \epsilon_F)$. $s_\sigma(T) = 1$ for all T here. The overall variation of ρ/ρ_* within a given T range increases with u and g . Hence, an appropriate choice of these parameters yields a resistivity which appears practically constant - c.f. e.g. the experimental data in ref.¹⁹ - although it has the same shape as the curves of fig. 3. Overall, the fit of eq. (14) is good. It can be seen that there is a discrepancy for low T . At the moment, we cannot determine the precise origin of this effect.

In fig. 4 we plot the magnetoresistance corresponding to eq. (14), as a function of (H/H_*) . The field at which $C_u = 0$ is $H_* = \sqrt{|1 - 2u + 3u^2/4|/(1 - u^2/4)}/(g_c \mu_B r)$, g_c the gyromagnetic ratio of the carriers and μ_B the Bohr magneton. Again, $s_\sigma(T) = 1$ for all T . The magnetoresistance for $H \rightarrow 0$ scales like (H^2/T^γ) , where $\gamma = 1.05$ for the parameter set (1) of fig. 3. The typical range of values of $\gamma \simeq 1$ are in marked difference from $\gamma_W = 2$ expected from the conventional weak disorder magnetoresistance, but compare very favorably with expts.²⁰.

Turning to the conventional weak disorder conductivity contributions in the presence of finite M , it is easy to see that they can typically be written as

$$\sigma_W = \frac{2e^2}{m^2} \int d\vec{k} k_x^2 \frac{\Gamma^2 W}{(1 - \Gamma M)^2} , \quad (15)$$

in a manner analogous to eq. (13) - but note the square in the denominator of eq. (15). W stands for any such diagrammatic contribution, with or without interactions. E.g. the conventional weak localization correction corresponds to $W \equiv -C$, $C_{q,\omega}$ being the Cooperon¹⁶. From eqs. (13) for σ_M and (15) for σ_W , we obtain $\sigma_W \ll \sigma_M$ for $W \ll M$. We believe this to be the explanation behind the negligible weak localization etc. contributions observed in a number of experiments^{19,21}. The same is true for the Hall coefficient as well, e.g.²¹. Note that, with increasing H , M decreases, and the weak disorder σ_W is enhanced, as seen in²¹. On the other hand, finite but small weak disorder contributions, which behave like $-\ln(T)$ in 2D^{16,2}, have also been observed in^{22,23}. In the frame of our model, it is reasonable to expect that at exponentially small T σ_W should dominate over σ_M , and hence drive the system into

the insulating regime. In that case, we would *not* have a $T = 0$ quantum metal-insulator phase transition. However, there are two caveats here. Kopietz has shown that the quasiparticle weight vanishes for $T \rightarrow 0^{24}$, in an interacting 2D Fermi gas with spinless disorder - the case with spin disorder remaining unresolved. Moreover, the well known Kohn-Luttinger instability to a superconducting phase may also interfere in the limit $T \rightarrow 0$. Hence the fate of the metallic state for $T \rightarrow 0$ is an open question.

Based on our model, we evaluate the specific heat δC_V of the carriers, corresponding to the same processes yielding σ_M in eq. (13). The free energy is

$$F_M = N_F \omega_o \tau K \ln \left(\frac{\epsilon_F - K\tau}{\epsilon_F + K\tau} \right) s_F(T), \quad (16)$$

with $K = \sqrt{g[z_1 F_1 + z_2 F_2]}$ and $\delta C_V = -T \partial^2 F_M / \partial T^2$. Here we took into account the diagrams of figs. 1 and 2. $s_F(T)$ has the same properties as $s_\sigma(T)$ above. As before, this result should not be valid for $T \rightarrow 0$. We note the pronounced H dependence of δC_V .

To summarize, we have shown that interactions and spin disorder can drive the second order metal-insulator transition observed in 2D systems. The transition arises from the onset of strong spin-density correlations, for a restricted range of the carrier density, the Zeeman energy and the temperature. We obtain good agreement with the experimentally determined dependence of the conductivity on these parameters.

I have enjoyed discussions and/or correspondence with P. Kopietz, P.T. Coleridge, A. Hamilton, E. Kiritsis, S.V. Kravchenko, V. Senz, S. Vitkalov and D. Williams. I acknowledge the hospitality of V.S. Vassiliadis in Cambridge.

APPENDIX A

Equations (3), derived in¹⁰, are standard Bethe-Salpeter equations in the spin-density channel, encompassing spin-scattering disorder and interactions. They are shown in fig. A1, and they form a complete system, containing *all* possible combinations of the interaction U and disorder lines in ladders, i.e. in the "no-crossing lines" approximation.

Their solution is given by

$$A^1 = U(1 - UD^{-1})/D_o, \quad A^0 = -U^2 \mathcal{D}^0 / D_o, \quad (17)$$

where the determinant D_o is

$$D_o = (1 - UD^{-1})(1 - UD^1) - (UD^0)^2. \quad (18)$$

To obtain the solution, we substitute \mathcal{D}^i according to the expressions given in the text. We perform the polynomial expansions in q^2, ω_m, ω_H in both numerator and denominator of the expressions resulting from eqs. (17), after writing common denominators which are products of all relevant denominators coming from the \mathcal{D}^i 's. Then, taking the limit $Dq^2 < \omega_m$, yields the solutions in eq. (4). The solutions in the opposite limit $Dq^2 > \omega_m$ can be found in¹⁰.

APPENDIX B

In this Appendix we calculate the basic diagrammatic block B of fig. 1

$$B = T^4 \sum_{\{\epsilon_1, \omega_1, \epsilon_2, \omega_2\} \{k_1, p_1, q_1, k_2, p_2, q_2\}} G(k_1, \epsilon_1) G(k_1 - q_1, \epsilon_1 - \omega_1) G(p_1, \epsilon_1) G(k - q_1, \epsilon + \Omega - \omega_1) \quad (19)$$

$$G(k_2, \epsilon_2) G(k_2 + q_2, \epsilon_2 + \omega_2) G(p_2, \epsilon_2) G(k + q_2, \epsilon + \omega_2)$$

$$A^j(q_1, \omega_1) A^j(k' - k + q_1, \epsilon' - \epsilon + \omega_1) A^{j'}(q_2, \omega_2) A^{j'}(k'' - k + q_2, \epsilon'' - \epsilon + \omega_2) D^{l, m_l}(k_1 - k_2, \epsilon_1 - \epsilon_2).$$

Here the indices l, m_l depend on j and j' . All the energies are Matsubara energies, but we suppress the usual indices m, n for the moment. The Green's function is $G(k, \epsilon_n) = 1/\{i\epsilon_n - \epsilon_k + i\text{sign}(\epsilon_n)/(2\tau)\}$. Fixing the external momenta and energies so that

$$k' = k'' = k, \quad \epsilon' = \epsilon'' = \epsilon, \quad (20)$$

the labels k, ϵ appear in both left and right external lines of the diagram. Thus the diagram can be inserted in a conductivity bubble, and calculate the conductivity accordingly. I.e. as a lowest order approximation - c.f. eq. (13) for the full formula - B can contribute to the conductivity through the formula

$$\sigma_1 = \frac{2e^2}{m^2} \int d\vec{k} k_x^2 (G_R(k, \epsilon_F) G_A(k, \epsilon_F))^2 B . \quad (21)$$

Eq. (20) implies directly that the two pairs of the interaction propagators $A^j(q, \omega)$ - corresponding to the upper and lower bubbles - have identical arguments. This gives rise to the resonance factors referred to in the text - c.f. the discussion around eq. (6) and R_j below. Equivalently, taking identical arguments for each pair of $A^j(q, \omega)$'s, yields eq. (20).

In fact, the resonance in question *selects* identical arguments q, ω for each pair of $A^j(q, \omega)$'s in diagrams of the type of B above, in which this is possible. In general, one can construct other diagrams, similar in structure to B, that is with pairs of $A^j(q, \omega)$'s connected to a common bubble, but in these instances it is *impossible* to obtain identical arguments q, ω for the two $A^j(q, \omega)$'s. These diagrams present no special interest, as they contain no resonance factors, and are omitted.

Also, eq. (20) implies that

$$p_1 = k_1 , \quad p_2 = k_2 . \quad (22)$$

Moreover, we can omit the $q_1, \omega_1, q_2, \omega_2$ dependence of the two Green's functions in the external part of the two bubbles.

Taking all this into account we can write

$$B = G_R(k, \epsilon) G_A(k, \epsilon) |R_j R_{j'}| \sum_q D^{l, m_l}(q, \omega_T) , \quad (23)$$

where

$$R_j = T^2 \sum_{0 < \omega_m, 0 < \epsilon_n < \omega_m, k, q} (A^j(q, \omega_m))^2 G^2(k, \epsilon_n) G(k - q, \epsilon_n - \omega_m) , \quad (24)$$

and we take ω_T as the smallest non-zero Matsubara energy difference

$$\omega_T = 2\pi T . \quad (25)$$

For the q summations we take $Dq^2 < \tau^{-1}$. Then,

$$\sum_q D^{j, m_j}(q, \omega_T) = \frac{F_{1,2}}{8\pi^2 \tau^2 N_F D} , \quad (26)$$

where the functions $F_{1,2}$ appear after eq. (11) and F_1 corresponds to $D^{0,0}$, while F_2 to $D^{1,1}$ - c.f. eq. (10) for D^{j, m_j} .

APPENDIX C

In this Appendix we evaluate the factor R_j . We see that

$$R_j = T \sum_{\omega_m, q} (A^j(q, \omega_m))^2 F(q, \omega_m) , \quad (27)$$

with

$$F(q, \omega_m) = T \sum_{k, 0 < \epsilon_n < \omega_m} G_R^2(k, \epsilon_n) G_A(k - q, \epsilon_n - \omega_m) . \quad (28)$$

We can omit the q -dependence in $F(q, \omega_m)$, $q < 1/\sqrt{D\tau}$ being much smaller than the relevant momenta of order k_F in $G(k, \epsilon)$, and then we evaluate

$$\begin{aligned} I(k, \omega_m) &= T \sum_{0 < \epsilon_n < \omega_m} G_R^2(k, \epsilon_n) G_A(k, \epsilon_n - \omega_m) \\ &= \frac{1}{2\pi i} \int_{-\infty}^{\infty} d\epsilon n_F(\epsilon) [G_R^2(k, \epsilon) G_A(k, \epsilon - i\omega_m) - G_R^2(k, \epsilon + i\omega_m) G_A(k, \epsilon)] . \end{aligned} \quad (29)$$

$n_F(\epsilon)$ is the Fermi-Dirac occupation function, and for low T we have

$$2\pi i I(k, \omega_m) \simeq \int_{-\infty}^{\epsilon_F} d\epsilon \left\{ \frac{1}{(\epsilon - \epsilon_k + it)^2} \frac{1}{\epsilon - i\omega_m - \epsilon_k - it} - \frac{1}{(\epsilon + i\omega_m - \epsilon_k + it)^2} \frac{1}{\epsilon - \epsilon_k - it} \right\} \quad (30)$$

$$= \frac{1}{\omega_m + 2t} \left\{ \frac{1}{\epsilon_F + i\omega_m - \epsilon_k + it} - \frac{1}{\epsilon_F - \epsilon_k + it} + \frac{i}{\omega_m + 2t} \ln \left(\frac{(\epsilon_F - \epsilon_k)^2 + t^2}{(\epsilon_F - \epsilon_k)^2 + (\omega_m + t)^2} \right) \right\}.$$

$t = 1/(2\tau)$. Subsequently

$$F(\omega_m) = N_F \int_0^{\infty} d\epsilon_k I(k, \omega_m) \quad (31)$$

$$= \frac{1}{2\pi} \frac{1}{\omega_m + 2t} \left\{ \ln \left(\frac{\epsilon_F + i\omega_m + it}{\epsilon_F + it} \right) + \frac{i}{\omega_m + 2t} \left[-2(\omega_m + t) \arctan \left(\frac{\omega_m + t}{\epsilon_F} \right) + 2t \arctan \left(\frac{t}{\epsilon_F} \right) + \epsilon_F \ln \left(\frac{\epsilon_F^2 + (\omega_m + t)^2}{\epsilon_F^2 + t^2} \right) \right] \right\}.$$

In the limit

$$\omega_m \ll t \ll \epsilon_F \quad (32)$$

of interest here, we obtain

$$F(\omega_m) = \frac{N_F \omega_m}{4\pi \epsilon_F^2}. \quad (33)$$

With $F(\omega_m)$ in hand, we proceed to calculate

$$Y(\omega_m) = \sum_q (A^j(q, \omega_m))^2 = \frac{1}{4\pi D} \int_0^{\omega_m} (A^j(x = Dq^2, \omega_m))^2 dx \quad (34)$$

$$= \frac{1}{4\pi D} \left\{ -\frac{1}{A_j^3} \frac{[A_u(K_{uj} + M_{uj}|\omega_m|) - L_{uj}(C_u + B_u|\omega_m|)]^2}{C_u + B_u|\omega_m| + A_u x} + Y_i \right\} \Big|_{x=0}^{x=\omega_m},$$

where we restrict ourselves to the dynamic limit $Dq^2 < \omega_m$.

$$Y_i = \frac{1}{A_u^3} \{ A_u L_{uj}^2 x + 2L_{uj}[A_u(K_{uj} + M_{uj}|\omega_m|) - L_{uj}(C_u + B_u|\omega_m|)] \ln(C_u + B_u|\omega_m| + A_u x) \}, \quad (35)$$

is an irrelevant term, which does not yield a significant contribution compared to the pole of $Y(\omega_m)$ - despite the logarithmic singularity - and will be omitted.

Subsequently we evaluate

$$R_j = T \sum_{\omega_m > 0} Y(\omega_m) F(\omega_m) = -T \sum_{\omega_m > 0} \frac{F(\omega_m)}{4\pi D A_u^3} \frac{[A_u(K_{uj} + M_{uj}\omega_m) - L_{uj}(C_u + B_u\omega_m)]^2}{C_u + B_u\omega_m} \quad (36)$$

$$\simeq \frac{TN_F \omega_o (K_{uj} + M_{uj}\omega_o)^2}{16i\pi^2 d \epsilon_F^2 A_u D},$$

where we approximated the ω_m sum by the term most closely located to the pole $\omega_m = \omega_o$ - c.f. eq. (6) - as $C_u < 0$ and $B_u > 0$, and we omitted the term in eq. (34) with $x = \omega_m$, as it yields a resonance at lower $\{\omega_o, \omega_o\}$ than in eq. (6).

* Current address. E-mail : kast@iesl.forth.gr

¹ S.V. Kravchenko, G. V. Kravchenko, J. E. Furneaux, V. M. Pudalov, and M. D'Iorio, Phys. Rev. B **50**, 8039 (1994); S.V. Kravchenko, W. E. Mason, G. E. Bower, J. E. Furneaux, V. M. Pudalov, and M. D'Iorio, Phys. Rev. B **51**, 7038 (1995); S.V. Kravchenko, D. Simonian, and M. P. Sarachik, Phys. Rev. Lett. **77**, 4938 (1996).

- ² E. Abrahams, S.V. Kravchenko & M.P. Sarachik, Rev. Mod. Phys. **73**, 251 (2001).
- ³ A.R. Hamilton, M. Y. Simmons, M. Pepper, E. H. Linfield, P. D. Rose, and D. A. Ritchie, Phys. Rev. Lett. **82**, 1542 (1999).
- ⁴ V.M. Pudalov, G. Brunthaler, A. Prinz & G. Bauer, Phys. Rev. B **60**, R2154 (1999).
- ⁵ V.M. Pudalov, JETP Lett. **66**, 175 (1997).
- ⁶ S. Ilani, A. Yacoby, D. Mahalu, H. Shtrikman, Phys. Rev. Lett. **84**, 3133 (2000).
- ⁷ S.C. Dultz, H.W. Jiang, Phys. Rev. Lett. **84**, 4689 (2000).
- ⁸ S.A. Vitkalov, H. Zheng, K. M. Mertes, M. P. Sarachik and T. M. Klapwijk, cond-mat/0008456.
- ⁹ S. Ilani, A. Yacoby, D. Mahalu & H. Shtrikman, Science **292**, 1354 (2001).
- ¹⁰ G. Kastinakis, Europhys. Lett. **42**, 345 (1998).
- ¹¹ The opposite limit $Dq^2 > \omega$ does not yield the effect sought for, despite $B_u < 0$ for $1 < u < 1.2$.
- ¹² M.P. Sarachik, S.V. Kravchenko, Proc. Natl. Acad. Sci. USA **96**, 5900 (1999).
- ¹³ C. Chamon, E.R. Mucciolo & A.H. Castro Neto, Phys. Rev. B **64**, 245115 (2001).
- ¹⁴ The value $\xi = 1$ yields a first order transition.
- ¹⁵ A. Völker & P. Kopietz, Phys. Rev. B **65**, 045112 (2002).
- ¹⁶ B.L. Al'tshuler & A.G. Aronov, in *Electron-Electron Interactions in Disordered Systems*, A.L. Efros, M. Pollak, Eds. (Elsevier, Amsterdam 1985).
- ¹⁷ $s_\sigma(T)$ appears as follows. The resonances of the pole of $A^j(q, \omega_m)$ occur at $T = T_m \equiv T_o/m$, with $m = 1, 2, 3, \dots$. This would yield a metallic state for this discrete set of T_m 's only. However, due to disorder inhomogeneity, both u and τ_S^{-1} vary in space, which we account for via an appropriate distribution of T_o , centered e.g. at T_o^* . The latter yields a *continuum* of relevant T_m 's, i.e. a metallic state for $T < T_o^*$ weighted by $s_\sigma(T)$.
- ¹⁸ To see this, consider any term of the conductivity series of eq. (13). By removing the current vertices we obtain the corresponding (generating) free energy diagrams of the approximation - c.f. G. Baym, Phys. Rev. **127**, 1391 (1962). Then, it turns out that the only possible way to generate conductivity diagrams, by inserting two current vertices, so that they contain diffusons etc., yields precisely the original diagrams of eq. (13).
- ¹⁹ S.V. Kravchenko & T.M. Klapwijk, Phys. Rev. Lett. **84**, 2909 (2000).
- ²⁰ V.M. Pudalov, G. Brunthaler, A. Prinz and G. Bauer, cond-mat/0103087; V.M. Pudalov, M.E. Gershenson, H. Kojima, G. Brunthaler, A. Prinz and G. Bauer, cond-mat/0205449.
- ²¹ P.T. Coleridge, A.S. Sachrjda & P. Zawadzki, cond-mat/9912041.
- ²² M.Y. Simmons, A. R. Hamilton, M. Pepper, E. H. Linfield, P. D. Rose, and D. A. Ritchie, Phys. Rev. Lett. **84**, 2489 (2000).
- ²³ V. Senz, T. Ihn, T. Heinzl, K. Ensslin, G. Dehlinger, D. Grutzmacher, and U. Gennser, Phys. Rev. Lett. **85**, 4357 (2000).
- ²⁴ P. Kopietz, Phys. Rev. Lett. **81**, 2120 (1998); also L. Bartosch & P. Kopietz, Eur. Phys. J. B **28**, 29 (2002).

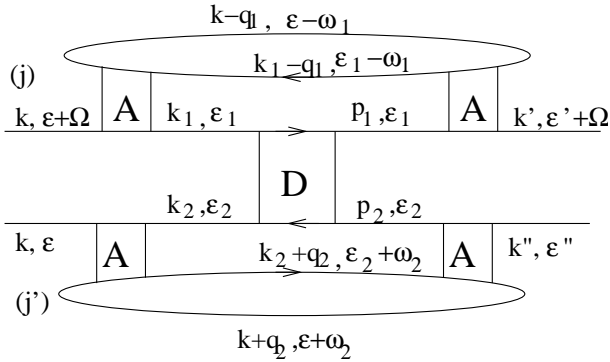


Fig. 1

The basic (lowest order) diagrammatic block for M_σ . $D_{q,\omega}$ is the diffuson and A the renormalized propagator of eq. (4). All the appropriate spin structure diagrams are kept.

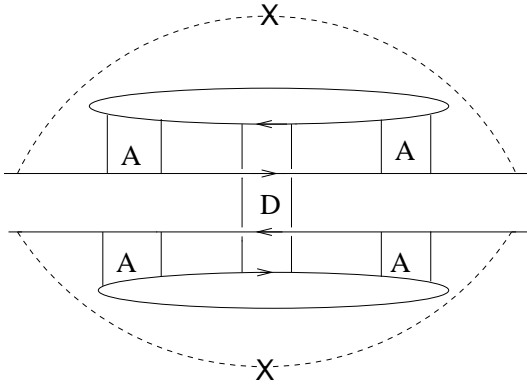


Fig. 2

Variations on the diagram of fig. 1. Here the diffuson connects the bubble lines. One or two impurity scattering line(s) decorate the main upper and/or lower line(s).

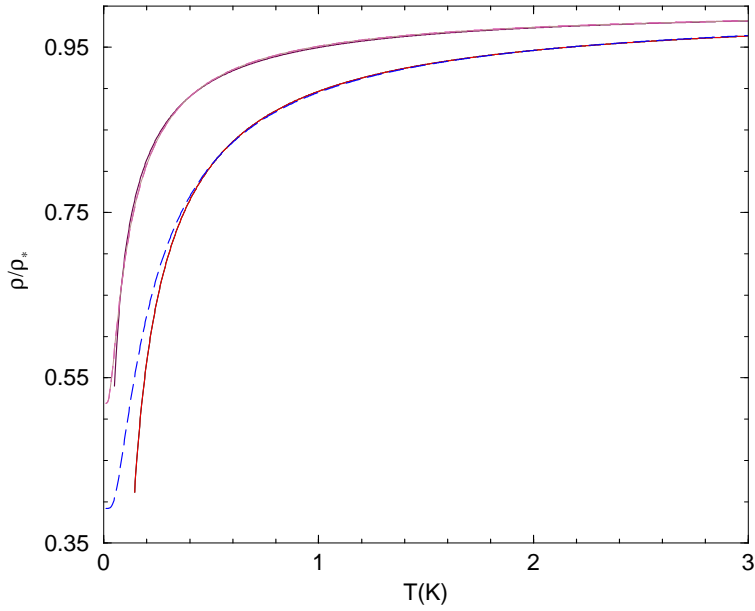


Fig. 3

Fit of eq. (14) - continuous lines - to the experimentally determined resistivity form of eq. (1) - dashed lines. Here $H = 0$ and $\rho_* = 3m\tau/(\pi e^2 N_F \epsilon_F)$. $\chi = 1$ and $\xi = 0$. Both lower (1) and upper (2) curves have $u=0.83$, $r = \tau^{-1} = 2$ K, and only differ by the ratio $g^{(1)}/g^{(2)} = 2$. The parameters of eq. (1) are $(\rho_o/\rho_*) = 0.392/0.519$, $(\rho_1/\rho_*) = 0.61/0.48$, $T_* = 0.192/0.1$ K and $k = 1/0.98$, for curves (1) and (2) respectively.

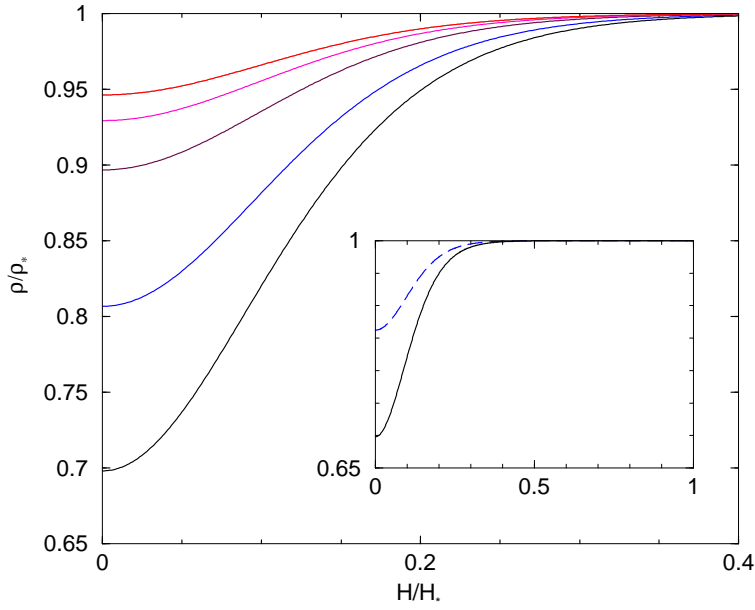


Fig. 4

Magnetoresistance from eq. (14), for the parameter set (1) of fig. 3. H_* is given in the text. The curves bottom to top correspond to $T=0.3, 0.5, 1, 1.5$ and 2 K. We note that $\rho/\rho_* = 1$ implies $M = 0$. The full curves to $H = H_*$ for $T = 0.3$ K are shown in the inset, the dashed line corresponding to the parameter set (2) of fig. 3.

$$\begin{array}{c}
 \begin{array}{c} \uparrow \quad \uparrow \\ \hline \overrightarrow{A^1} \\ \hline \downarrow \quad \downarrow \end{array} = U \begin{array}{c} \uparrow \\ \hline \hline \hline \downarrow \end{array} U \begin{array}{c} \uparrow \quad \uparrow \quad \uparrow \quad \uparrow \\ \hline \overrightarrow{D^1} \quad \overrightarrow{A^1} \\ \hline \downarrow \quad \downarrow \quad \downarrow \quad \downarrow \end{array} + U \begin{array}{c} \uparrow \quad \downarrow \quad \uparrow \\ \hline \overrightarrow{D^0} \quad \overrightarrow{A^0} \\ \hline \downarrow \quad \uparrow \quad \downarrow \end{array} \\
 \\
 \begin{array}{c} \downarrow \quad \uparrow \\ \hline \overrightarrow{A^0} \\ \hline \uparrow \quad \downarrow \end{array} = U \begin{array}{c} \downarrow \quad \uparrow \quad \uparrow \quad \uparrow \\ \hline \overrightarrow{D^0} \quad \overrightarrow{A^1} \\ \hline \uparrow \quad \downarrow \quad \downarrow \end{array} + U \begin{array}{c} \downarrow \quad \downarrow \quad \uparrow \\ \hline \overrightarrow{D^{-1}} \quad \overrightarrow{A^0} \\ \hline \uparrow \quad \uparrow \quad \downarrow \end{array}
 \end{array}$$

Fig. A1

The Bethe-Salpeter eqs. (3). The thin double line stands for U . The factors \mathcal{D}^i are given in the text. Note the explicit spin indices of the various components of the diagrams.